11th AIAA Aviation Technology, Integration, and Operations (ATIO) Conference, including the AIA
20 - 22 September 2011, Virginia Beach, VA

AIAA 2011-6918

Assessing and Estimating Risk of Operating Unmanned Aerial Systems in Populated Areas

Christopher W. Lum,[*] Kristoffer Gauksheim,[†] Tadej Kosel,[‡] and Tad McGeer[§]

Autonomous Flight Systems Laboratory

University of Washington, Seattle, WA, 98195, USA

In order to operate in the national airspace, an aircraft system must have documentation and analysis to show that it can operate at a satisfactory level of safety. For traditional manned aircraft systems, this is equivalent to operating a reliable system. However with Unmanned Aerial Systems (UAS), a relatively unreliable system can safely be operated provided that the risk to bystanders on the ground is sufficiently low. This paper presents a set of design tools and methodologies which can be used to assess the risk associated with operating an UAS in a potentially populated area. The intended use of the tool is discussed and a risk assessment is provided for an existing UAS.

Nomenclature

ADS-B	Automatic Dependent Surveillance-Broadcast
$A_{L_H p}$	Lethal area for pedestrians in a horizontal crash (due to system failure) (km^2)
d	Horizontal distance traveled during a failure (m)
D	Protection factor between aircraft and human (in range $[0, 1]$)
$\tilde{F}_{fat}$	Number of fatalities for a given failure (fatalities)
F_{fat}	Total fatalities due to system failures (fatalities/hour)
h	Height of aircraft at time of failure (m)
H_p	Average pedestrian height (km)
L_{ua}	Length of UA (km)
MOA	Military Operating Area
NAS	National Airspace
$p(x, y)$	Continuous probability density function of crash
$p_d(x, y)$	Discrete probability density function of crash
SAA	Sense and Avoid
TBO	Trajectory Based Operations
UA/UAS	Unmanned Aircraft/Unmanned Aerial System
w_{ua}	Wingspan of UA (km)
γ	Glide angle of UA at failure (radians)
λ	UAS midair failure rate for a single AC (failures/hour)
σ_p	Pedestrian densities (items/km^2)
θ	Average glide angle during a failure (rad)

I.   Introduction

In the future, Unmanned Aerial Systems (UAS) will interact with general aviation and commercial flights in many different ways. They will bring with them new technologies and new possibilities in terms of missions

---

[*]Research Scientist, Dept. of Aeronautics and Astronautics, University of Washington, lum@u.washington.edu
[†]Research Assistant, Dept. of Aeronautics and Astronautics, University of Washington, krg@u.washington.edu
[‡]Associate Professor, Dept. of Aviation, University of Ljubljana, tadej.kosel@fs.uni-lj.si
[§]Founder, Aerovel Corporation, tad@aerovelco.com

that could be achieved. UAS will have to respect restrictions and constraints imposed by the Federal Aviation Administration (FAA) in order to achieve an acceptable level of safety and security. Usage of UAS by military organizations around the world has increased dramatically in the last several years. However, growth of UAS in the civilian and commercial market has been markedly slower. This is especially true in the U.S. where concerns over safe integration and operation of UAS in the national airspace system (NAS) have restricted the accessibility of this market. One of the main restrictions is the ambiguous and non-standardized set of design tools and methodologies which are currently employed by various UAS manufacturers in order to assess risk of a mission. This paper documents the development of a simplified model to assess and predict risk associated with a given UAS operation. This tool is intended to be useful for determining UAS scenarios that can operate at an acceptable level of safety from the perspective of risk to human safety.

Several efforts have been made in the past to assess the risk of a UAS mission. One of the first efforts involved modeling mid-air collisions of manned aircraft using random collision theory and comparing results to historical data by Anno.[1] Similar work was performed by McGeer[2] with extensions involving regulatory policy and economics of these systems.[3]

More recently, focus has shifted towards integrating UAS into the NAS.[4] A similar risk-based approach to analyzing the safety of UAS operations was taken by Burke[5] at North Carolina State University in the development of the System Level Airworthiness Tool (SLAT). The author also chose to focus on the expected number of fatalities per flight hour as the primary safety metric. A similar approach was taken by Waggoner[6] and Lum[7] when developing a design tool to allow the risk associated with a given UAS mission to be calculated.

The current work focuses on building from many of these previously stated ideas in order to develop a methodology which can be used by UAS manufacturers when evaluating the risk of testing their systems in potentially populated areas. The example used in this paper focuses on performing a risk assessment required to obtain an Experimental Type Certificate for the Flexrotor aircraft[8] to perform flight tests near Husum, WA. The main metric for safety is potential harm to bystanders on the ground. Previous results[7] have shown that the vast majority of failures of UAS are due to general system failures rather than mid-air collisions. Therefore, the primary concern is that when a UA fails, it will strike someone on the ground and cause harm.

Additional references and prior work are presented in the context of the federal UAS policy in Section II. This section serves as motivation by looking at current US policy relevant to UAS operations. Section III then describes some of the framework used to develop the overall risk model. Results and example calculations of this scenario are presented as well. Finally, Section IV presents conclusions and future directions of research.

II.   Current UAS Policy

Without a thorough understanding of the risks involved, regulations on the flight of UAS in US airspace have thus far been highly prohibitive. Policy was set forth in a September, 2005 Federal Aviation Administration (FAA) memorandum,[9] clarified in a 2006 notice,[10] and replaced in March 2008 by the Interim Operational Approval Guidance.[11] Currently, the only avenue to receive approval of civil (i.e. commercial, academia) UAS operation is through a special experimental airworthiness certificate. The special certificate is subject to operational limitations (e.g. line of sight operation, daylight hours, etc.) and is only issued "for the purposes of research and development, crew training, or market survey." The procedure and guidelines for issuing a special experimental certificate are detailed by the FAA.[12]

A second avenue, a certificate of authorization (COA), was closed to civil applications in 2005 by FAA memorandum AFS-400[9] but is still used for public (i.e. government/military) requests after the vehicle has been deemed airworthy by the FAA or DoD. A category that a minority of UAS may fall under is model aircraft[13] (strictly non-business related). Other documents of interests include NATO's UAV Systems Airworthiness Requirements[14] and the European Aviation Safety Agency's (EASA) statement on Airworthiness Certification of Unmanned Aircraft Systems.[15]

UAS policy is currently being reviewed to develop a long-term approach to a fluid integration of UAS into the NAS. Several components of the NextGen Air Transportation System (ATS) should help facilitate this process in the coming years.[16] NextGen refers to the next generation of the NAS being incrementally implemented over the course of several years, with current mid-term goals set through 2018. Two key NextGen technologies that have the greatest potential to impact UAS integration are Automatic Dependent Surveillance-Broadcast (ADS-B) and 4D Trajectory Based Operations (TBO).[17,4] The FAA's perspective

American Institute of Aeronautics and Astronautics

on UAS has been supportive but cautious as indicated by the following excerpt,[9]

> "The FAA supports UA flight activities that can demonstrate that the proposed operations can
> be conducted at an acceptable level of safety. AFS intends to approve COA applications... [if]
> a collision with another aircraft...is extremely improbable....[and] injury to persons or property
> along the flight path is extremely improbable. Acceptable system safety studies must include a
> hazard analysis, risk assessment, and other appropriate documentation that support the 'extremely
> improbable' determination."

A. Motivation

It is generally perceived that there are a number of obstacles to the full integration of UAS into the NAS. The most pressing technological challenges are "sense and avoid" (SAA) capability and command and control (C2) link liabilities.[4] Sense and avoid refers to the capability of an autonomous vehicle to detect objects, both stationary and mobile, that do not broadcast their position, which are in the vehicle's path (or otherwise on a collision course) and, if necessary, alter the vehicle's course to avoid a collision. Since the pilot of a UAS is not able to provide the "see and avoid" ability of an onboard pilot, the development of reliable SAA technology is believed to be essential for UAS to gain full airspace access. Significant work has been done both in R&D of SAA technologies and in establishing qualifications for an acceptable SAA system.[18]

Although most UA[a] will have low-level autonomy, a reliable communication link between the UA and the pilot is necessary for high-level control (navigation, tasking, air traffic control, etc.). In addition to improving the C2 link reliability, protocols must be developed to ensure safe and predictable behavior in the case of a lost-link. There is also much work to be done on the policy front. Guidelines are needed on airworthiness, crew training, operational protocols and how UAS will fit into the current and NextGen airspace structures.

Thoroughly addressing all of these issues, so that UAS may be routinely and safely incorporated throughout the NAS, will take years. In the mean time, standards and tools need to be developed that will, "enable the widest range of activity that can be safely conducted within the shortest rulemaking timeframe" (ASTM F38 Committee). Until new technologies are developed and a new system is in place, UAS operation approvals will continue to require mission specific risk assessments.

The purpose of the risk assessment tool presented in this paper is two-fold. First, it seeks to provide UAS operators and airspace regulators with a simplified and trustworthy method of evaluating the safety of proposed UAS operations. Tools are needed that provide UAS operators with "documentation that support the 'extremely improbable' determination," since it is an essential part of the current approval process. The availability of a tool to assess the risk of particular proposed UAS operation should make the process of obtaining approval more efficient and manageable.

The second objective is that the results of risk assessments performed using this tool would supply useful information to the aerospace community as future standards and guidelines are being developed. Successful regulation will prohibit unsafe operations while clearing the way for operations that do not pose a threat to public safety. Tools such as this risk assessment procedure will help determine what type of operations pose significant risk and which do not so that the policies being developed can reflect the risk associated with various UAS applications in order to maintain a high level of safety.

III. Design Tools and Methodology for Assessing Risk

The example aircraft used in this analysis is the Flexrotor manufactured by the Aerovel Corporation shown below in Figure 1(a).

The goal of this work is to assess the relative level of risk associated with operating this aircraft in the Husum, WA area (N45.8030^o W121.4823^o). This same methodology can be applied to other types of UAS in potentially populated areas.

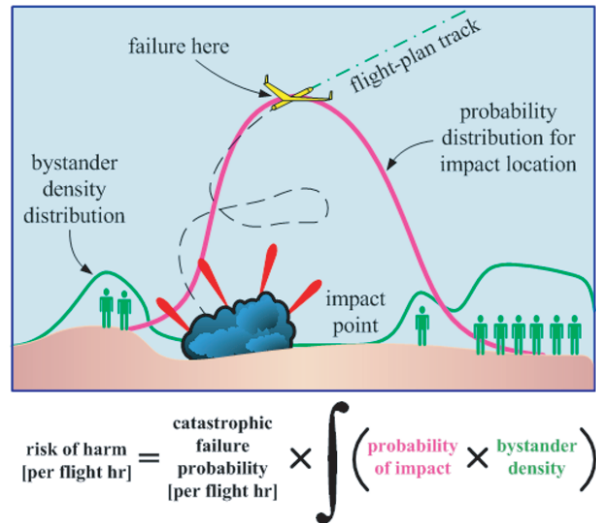## A. Experimental Type Certificate for Flexrotor

The first step to providing evidence to support the previously mentioned 'extremely improbable' determination is to understand and model how system failures ultimately correlate to human injuries and fatalities.

---

[a]UA is used to refer only to the aircraft, whereas UAS refers to the whole system inclusive of all ground-based equipment and any communication links.

American Institute of Aeronautics and Astronautics

(a) Flexrotor is a unique aircraft developed by Aerovel which is able to operate in both traditional wing-borne flight and hover in thrust-borne flight.

(b) General outline of risk assessment workflow for Flexrotor.

Figure 1. Flexrotor and workflow for paper.

Aerovel is in the process of performing the necessary analysis to obtain an experimental type certificate for flying aircraft in the national airspace. Being able to test the aircraft near the manufacturing facility has the potential to save on travel expenses and lost opportunity while waiting for access to restricted airspace such as the Boardman, OR test range. This analysis could serve as a model for acceptance of risk analysis by the FAA.

Risk analysis for Flexrotor involves introducing, in simulation, a catastrophic control failure at random during flight over the Elsner airfield in Husum, WA. The failure is then simulated to the point of impact. Thousands of such runs are easily done, and allows an estimate of the probability distributions for impact around the test site. Meanwhile, census data and satellite imagery is used to estimate the local bystander distribution. The estimated failure rate of the system is taken from experimental results and hardware-in-the-loop simulation. An estimate of the risk of harm to nonparticipants on the ground can then be calculated as shown in Figure 1(b).

B.   Failure Simulation

A major component of the risk assessment involves analyzing a large amount of failures of the aircraft and simulating impact zones and areas from these failures. A representative flight of the aircraft is first simulated and then state information is logged for this flight. The representative flight timeline is described in Table 1.

A failure is then injected to the flight at random times. The failure times are uniformly sampled from the representative flight. In order to simulate a flight computer failure, the control surfaces are frozen at their current state and the engine is shut down at a randomly selected time. The dynamics of the powerless aircraft are then propagated forward in time using a high fidelity, proprietary numerical simulator until the aircraft reaches a preset altitude of 178m (altitude of terrain near Husum, WA). A sampling of approximately 15,000 initial failure points are shown in Figure 2(a). Results of these forward simulations after failure are shown in Figure 2(b).

As can be seen, the vast majority of crashes occur very close to the initial failure location. This implies that once the aircraft experiences a failure, the system rapidly descends and crashes.

C.   Crash Probability Distribution

Because the failures are introduced at various altitudes, one useful normalizing parameter is the average glide angle between the initial failure point and the crash location. Geometry of the situation is shown in Figure 3.

American Institute of Aeronautics and Astronautics

Table 1. Timeline of representative Flexrotor flight at Husum, WA flight area.

Time (sec)	Action
0	Thrust-borne launch
5	5 m/s spanwise slew command to North
90	5 m/s spanwise slew command to South
165	Transition to wing-borne flight begins
177	Transition completes
177	Commanded to 678m altitude
178	Commanded to track 1200m x 300m box
250	Established on north-bound box leg
394	Commanded to 26m/s
493	Commanded to 31m/s
584	Commanded to 36m/s
654	Commanded to 41m/s
717	Commanded to 21.3m/s
735	Go direct to launch/retrieval point
789	Transition to thrust-borne flight begins
797	Transition complete
800	Commanded to 182m (4m AGL)
1135	Established at altitude
1140	Commanded 0.2m/s descent
1166	Touchdown
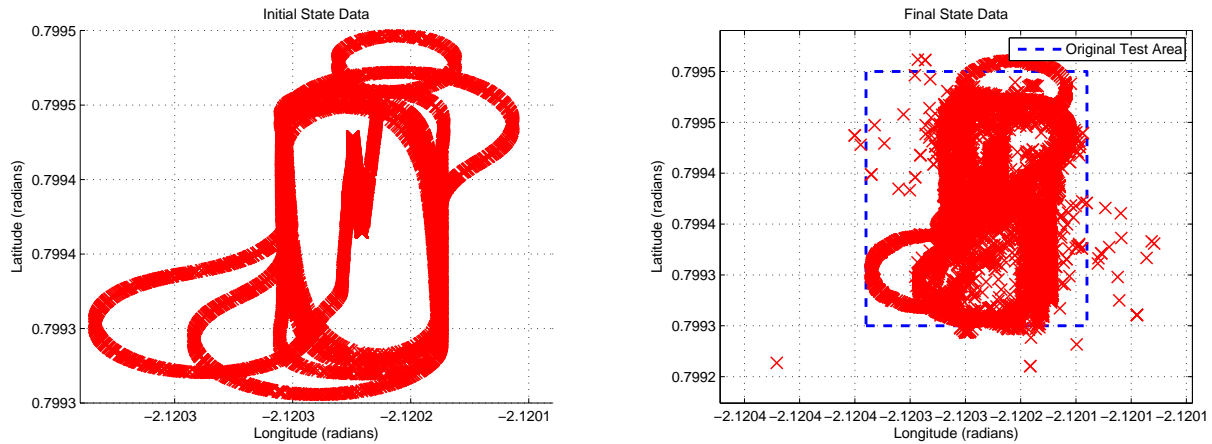
(a) Initial location of approximately 15,000 failures sampled uniformly from the representative flight. Representative flight is contained within an 800m wide (east to west) by 1500m tall (south to north) test area.

(b) Final state data showing location of aircraft crashes.

Figure 2. Impact distribution of aircraft with failures injected to representative flight.

From the geometry, the average glide angle is simply given by

$$\theta = \tan^{-1}(h/d) \tag{1}$$

A histogram of the average glide angle is shown in Figure 4(a). As can be seen from this histogram, the

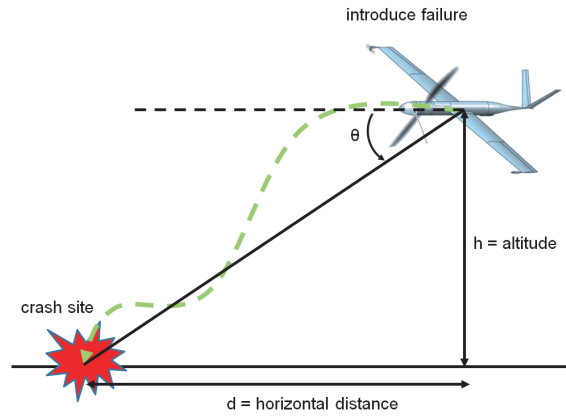American Institute of Aeronautics and Astronautics

Figure 3. Geometry showing average glide angle of aircraft between failure and crash site.

majority of glide angles are near 90 degrees, implying that most of the crashes occur near the location of the initial failure. The benefit of analyzing the glide angle is that it allows the radial distance traveled before crashing to be normalized by the altitude. For example, if a mission has the aircraft operating at an average altitude of h, for a given glide angle, the radial distance between failure and crash can be computed using Eq. 1 to obtain

$$d = h \cdot \tan(\theta) \qquad (2)$$

Eq. 2 can then be applied to the distribution shown in Figure 4(a) to obtain the distribution of horizontal distance between failure and crash for a nominal operation altitude of 500m. This histogram is shown in Figure 4(b).
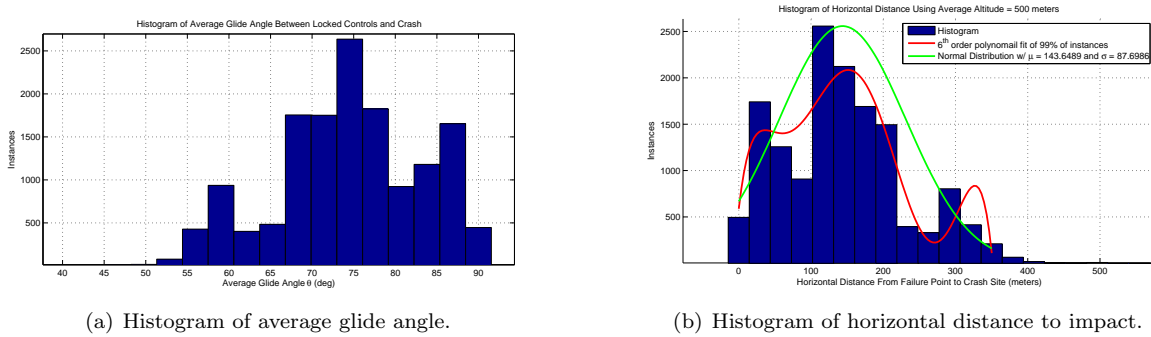
(a) Histogram of average glide angle.

(b) Histogram of horizontal distance to impact.

Figure 4. Histograms of relevant data obtained during Monte Carlo simulation of aircraft failures.

From this figure, one can see that the vast majority of crashes (99.97%) occur within 600m of the initial failure location. One method to parameterize this distribution is to fit a polynomial function to the histogram. To avoid a badly scaled polynomial, the tails of the histogram are not fitted, instead, a 6th order polynomial is used which fits 99% of the instances which are in the range of $d \in [0, d_{max}]$ where $d_{max} = 350m$. Physically, this means that 99% of all crashes happen within 350m of the failure point. This polynomial fit is determined to have the form of

$$f(d) = \sum_{k=0}^{6} a_k d^k \qquad (3)$$

The approximate values of the polynomial constants are shown in Table 2.

Note that $f(d)$ is not a probability density function (PDF). However, it can be converted to a PDF by normalizing it so that the area under the curve is one. Therefore, for a given failure, the PDF describing the

American Institute of Aeronautics and Astronautics

Table 2. Approximate constants for polynomial fit of histogram in Figure 4(b).

Parameter	Value	Parameter	Value	Parameter	Value
a_0	588.3	a_1	67.0	a_2	-1.9
a_3	0.02	a_4	-0.0001	a_5	0
a_6	-3.77×10^{-5}	-	-	-	-

horizontal distance traveled before impact likelihood in the range of $d \in [0, d_{max}]$ is given by

$$\tilde{p}(d) = \frac{1}{\gamma}f(d) \tag{4}$$

where $\gamma = \int_0^{d_{max}} f(\tau)d\tau$.

Therefore, the total PDF for an entire range of distances is given as

$$p(d) = \begin{cases} \tilde{p}(d) & d \in [0, d_{max}] \\ 0 & \text{otherwise} \end{cases} \tag{5}$$

Alternatively, a second method is to use a simple Gaussian/Normal distribution to fit the crash instances. The mean, μ, and standard deviation, σ, are found to be approximately 144 and 88 respectively. The alternative PDF is therefore given as

$$p(d) = \frac{1}{\sqrt{2\pi\sigma^2}}e^{\frac{-(d-\mu)^2}{2\sigma^2}} \tag{6}$$

Eq. 5 or Eq. 6 represent 1 dimensional functions which quantify the probability of a crash a certain distance from the crash origination point. By setting this point as the origin, these functions can be rotated around the origin to create a 2 dimensional PDF which covers a finite area around the flight test area.

$$\tilde{p}(x, y) = \frac{1}{\sqrt{2\pi\sigma^2}}\exp^{\frac{-(\sqrt{x^2+y^2}-\mu)^2}{2\sigma^2}} \tag{7}$$

Note that in Eq. 7, only the positive portions of the 1D PDF from Eq. 6 are rotated about the origin. Furthermore, note that a valid 2D PDF cannot be obtained by simply rotating a 1D PDF about a point. The function must be re-normalized to obtained a true 2D PDF as shown in Eq. 8.
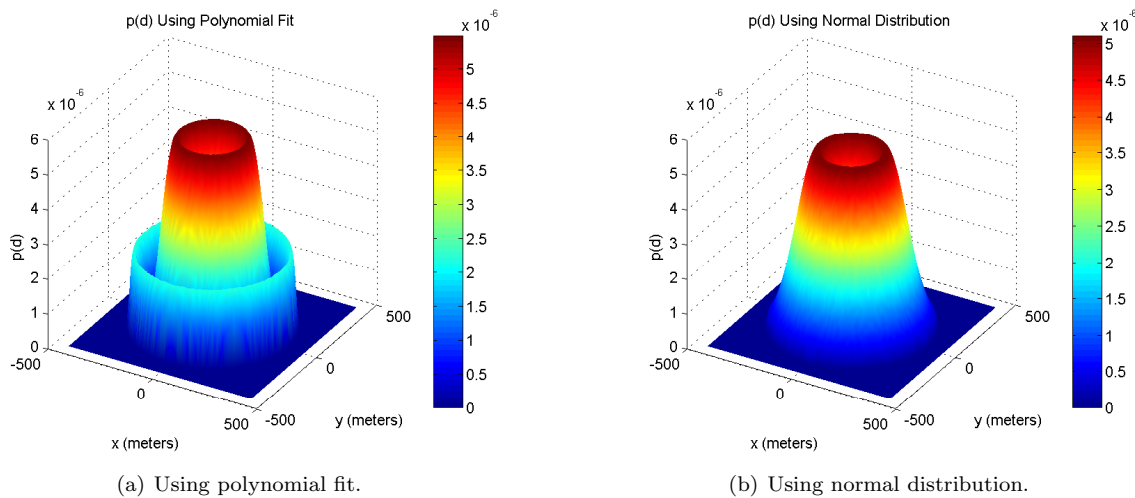
$$p(x, y) = \frac{\tilde{p}(x, y)}{\iint\limits_{-\infty}^{+\infty} \tilde{p}(x, y)\,\mathrm{d}x\,\mathrm{d}y} \tag{8}$$

Either the polynomial fit or the Normal distribution can be used in Eq. 8 as shown in Figure 5.

Notice that both representations yield somewhat multi-modal distributions (even the Gaussian distribution). This accurately reflects the fact that there is a low probability of a crash directly below the point of failure. This method can be used to fit alternative distribution functions if desired. Note that polynomial representation is highly dependable on coefficient accuracy. Because a small error in polynomial coefficient leads to a large error in functional accuracy, the remainder of the analysis focuses on the Gaussian representation shown previously in Eq. 6. Furthermore, the increased accuracy of the polynomial does not benefit the final result because of the large amount of approximations that have been made in other parameters and analysis.

D. Integration With Satellite Imagery

With traditional manned aircraft, any type of failure which results in a crash is likely to cause harm to human life (due to people on board the failed aircraft). However with UAS, the probability of injury or fatality due to an aircraft failure is highly dependant on the geographical location where the system is operating. Operations and subsequent failures in highly populated areas will likely result in higher levels of injury to

American Institute of Aeronautics and Astronautics

(a) Using polynomial fit.   (b) Using normal distribution.

Figure 5. 2 dimensional radial crash probability functions.

bystanders than operations in unpopulated rural areas. A satellite image of the flight test area near Husum, WA taken from Google Earth is shown in Figure 6.

In this figure, note that the flight test field is located at approximately $(200, -200)$ and the town of Husum is located in lower left corner of image. Also note that there are various features in this image such as roads and forests. These different type of areas likely have different population densities. For example, the population density in downtown Husum is likely much higher than that in the rural fields and forests. For the purpose of this analysis, each pixel of this image can be classified one of four categories, town, roads, forest, and fields. Various classifiers can be used to perform this operator. In this situation, a simple threshold based on image color is used with results shown in Figure 7.

Note that this pixel classification is note entirely accurate (for example, the red block near the origin is in fact a field instead of a road) but provides sufficient accuracy for this application. The population density of each class of pixel must now be assigned. For roads around the Husum area, the estimated traffic density is 10 cars per hour with an average of two people per car. The average speed is estimated as 60 km/hr. This means that the time between vehicles is approximately 6 minutes with a spacing of 6 km. The road is assumed to be 5 m wide, so the population density on the road is approximately 67 people/km^2.

For town areas, there are an estimated 5 people/building. The average projected area of the building is 100 m^2 yielding a population density of 50,000 people/km^2.

For forest, a population density of 10 people/km^2 is assumed and for fields, a population density of 20 people/km^2 is used.

The total area of the image shown in Figure 7 is determined to be 2.3246 km^2 and the area of a single pixel is 1.215 m^2. The composition of pixel percentages for roads, buildings, forest, and fields are approximately 6%, 2%, 44%, and 48%, respectively. However, knowing the breakdown of the various categories is not sufficient to determine bystander fatalities. As mentioned previously, if the aircraft fails over the highly populated town, the expected fatalities will be higher than if it fails over an unpopulated forest area. To quantify this, the crash PDF must be integrated with the classified satellite image. Flight test operations are centered at the origin of Figure 7. The combined PDF and satellite image is shown in Figure 8.

This allows a general idea of areas of high probability of collision. For example, the areas approximately 150 meters from the failure location are subject to higher crash probabilities than other areas (due to the mean of the distribution being $\mu \approx 150$ meters). The probability of a collision in each pixel can now be calculated. Consider the pixel defined by $x \in [x_{min}, x_{max}]$ and $y \in [y_{min}, y_{max}]$. Once the aircraft fails, the probability that it will crash in the given pixel is simply obtained by integrating Eq. 8 over this area

$$p(\text{crash in pixel}) = \int_{y_{min}}^{y_{max}} \int_{x_{min}}^{x_{max}} p(x, y)\, \mathrm{d}x\, \mathrm{d}y \tag{9}$$

Although this can be analytically solved with the desired normal distribution, for a general PDF (such

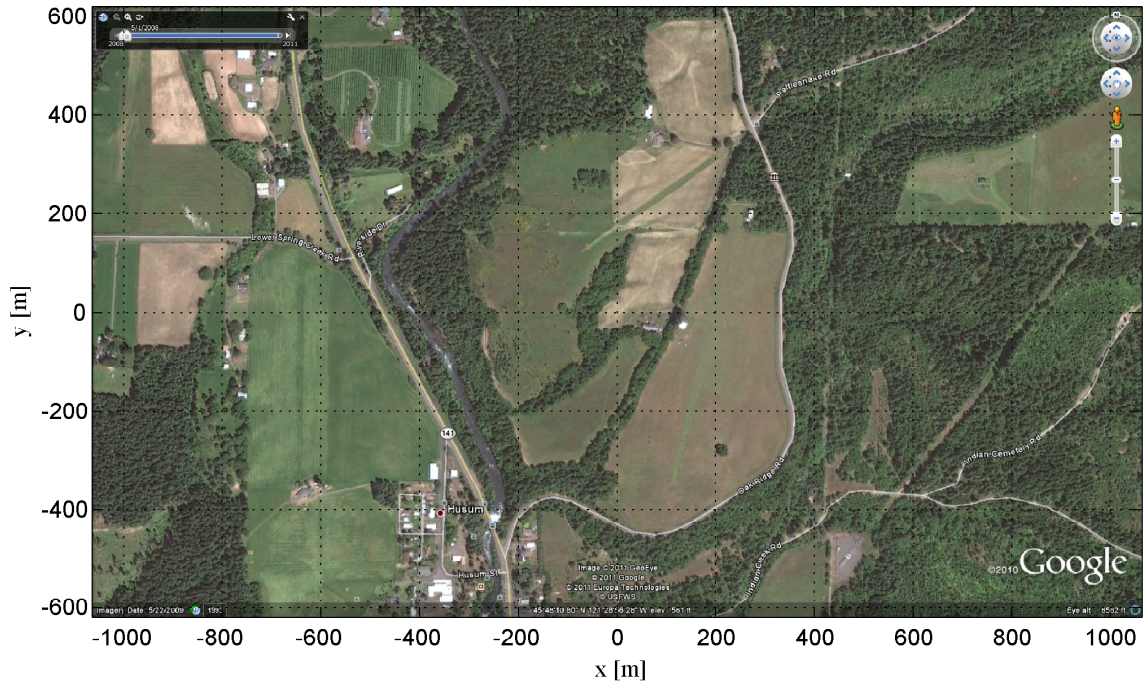American Institute of Aeronautics and Astronautics
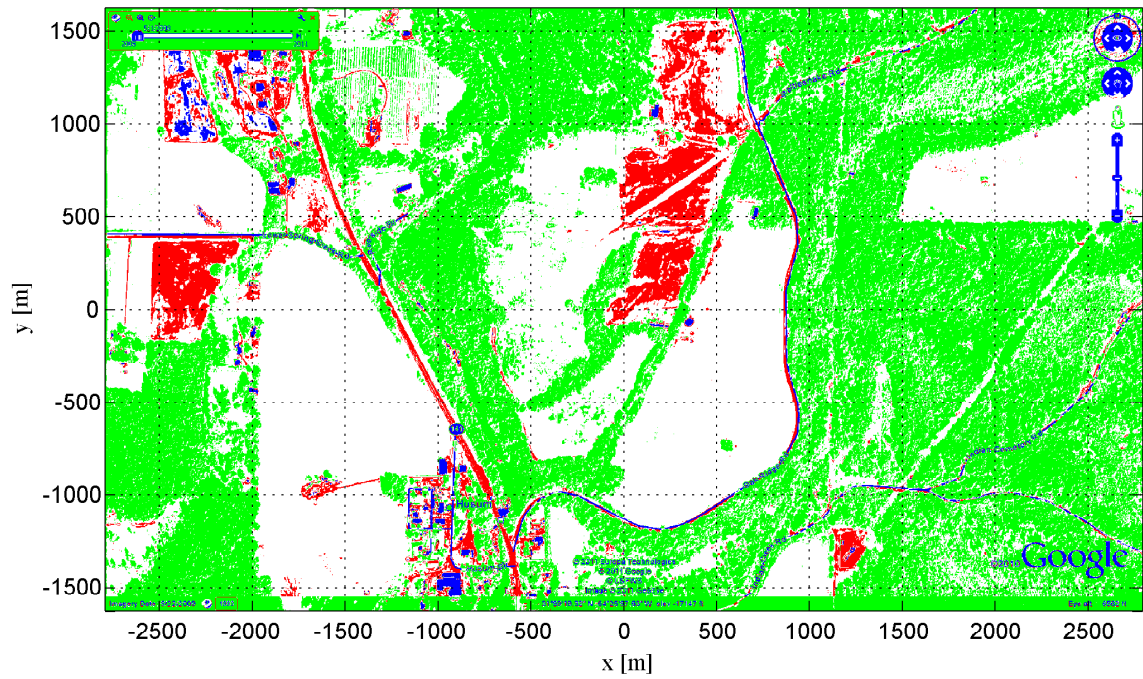
Figure 6. Satellite image of flight test area near Husum, WA.

Figure 7. Image showing each pixel classified as towns (blue), roads (red), forest (green), fields (white)
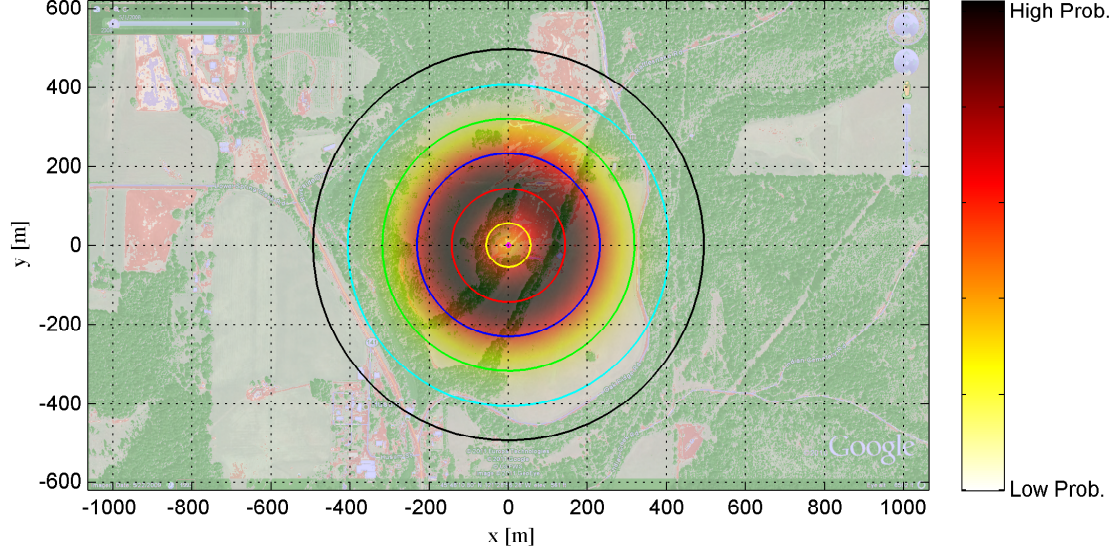
American Institute of Aeronautics and Astronautics

Figure 8. Population density near the Husum, WA flight test area combined with crash probability distribution.

as the polynomial or other type of fit), this integral may not be feasible to solve. Therefore, a discrete approximation of this continuous PDF can be computed such that the discrete probability of crashing within a given pixel is directly proportional to the continuous PDF value at the center of the pixel.

$$p_d(\text{crash in pixel}) \propto p(x_{max} + \frac{x_{max} - x_{min}}{2}, y_{max} + \frac{y_{max} - y_{min}}{2}) \tag{10}$$

Algorithmically, the discrete probability density function, $p_d(x,y)$ is computed by computing the location of all pixel centers, evaluating the continuous PDF, $p(x,y)$, at this location, and then renormalizing the discrete PDF such that $\sum_i \sum_j p_d(x_i, y_j) = 1$.

Once the aircraft fails, it is assumed that the UAS will glide and potentially strike pedestrians on the ground. The lethal areas where pedestrians may be struck is illustrated in Figure 9.

The potentially lethal area is given as

$$A_{L_{Hp}} = (w_{ua} + 2R_p)(L_{ua} + \frac{H_p}{\tan \gamma} + 2R_p) \tag{11}$$

Therefore, with a given population density of σ_p, the expected number of collisions is simply the product of $A_{L_{Hp}}$ and σ_p (note that σ_p is a function of the type of pixel). In order to map collisions into fatalities, a protection factor, D, is incorporated to model the fact that a failure and collision between the UAS and a car on a road is less likely to generate a fatality than when the same UAS collides with a pedestrian in an open field). This value of D ranges from 0 (to model no protection and a collision always results in a fatality) to 1 (modeling a fully protected individual, for example inside a hardened bunker). Therefore, given a failure, the expected number of fatalities is given as

$$\tilde{F}_{fat} = A_{L_{Hp}} \sigma_p (1 - D) \tag{12}$$

Eq. 12 can be applied to each pixel and combined with the UAS expected mean time between failures, λ, to obtain the final, total number of expected fatalities per flight hour as

$$F_{fat} = \lambda \sum_i \sum_j p_d(i,j) \tilde{F}_{fat} \tag{13}$$

Note that in Eq. 13, many of the terms in $\tilde{F}_{fat}$ are a function of the pixel location and type. This formulation is based on previously work regarding midair collisions and general system failures.[7]

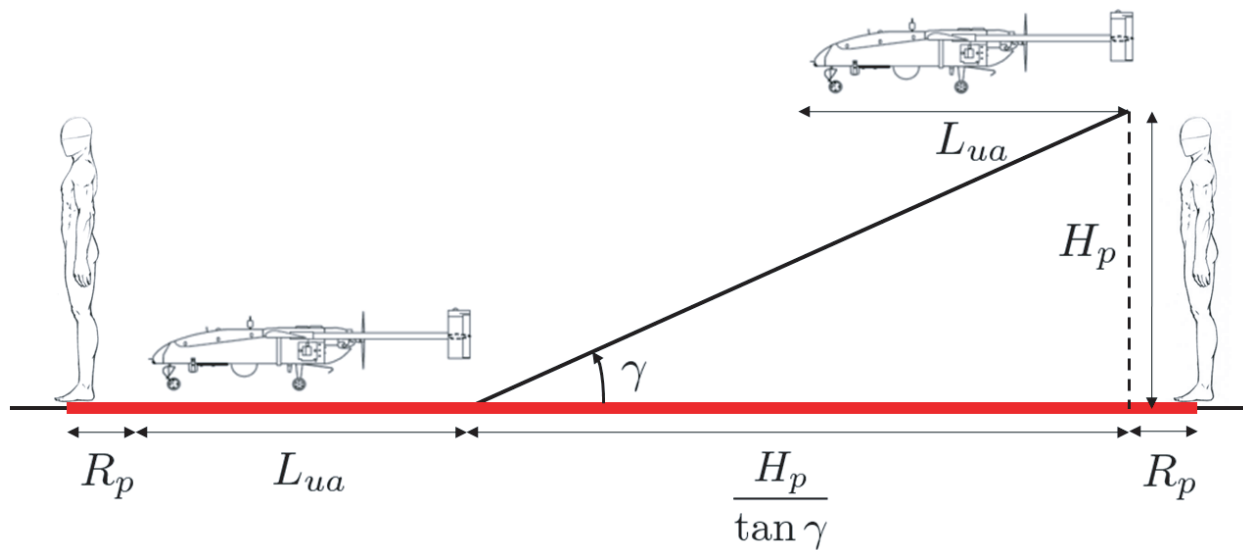American Institute of Aeronautics and Astronautics

Figure 9. Geometry showing affected distance covered by UA during a horizontal, gliding crash (red distance). The total affected areas is this distance multiplied by the wingspan of the UA plus $2R_p$.

Table 3. Parameters used to estimate human collison/hr for this scenario.

Parameter	Value	Comment
λ	0.1	UAS midair failure rate for a single UA (failures/hr)
γ	variable	Glide angle upon failure. Computed based on pixel location
w_{ua}	3m	Wingspan of UAS
L_{ua}	1.6m	Length of UAS
R_p	0.25	Radius of person
H_p	1.8m	Height of person
σ_p	variable	Population density (67 for roads, 50,000 for towns, 10 for forest, 20 for fields)
D	variable	Protection factor (0.5 for roads, 0.5 for towns, 0.1 for forest, 0 for fields)

Some other relevant parameters used to estimate the human collisions/hr are shown in Table 3.

The results of the analysis yield that the fatality rate for forest, roads, towns, and fields are approximately 1.5E-5, 3.5E-6, 6.7E-5, 1.4E-5 fatalities per hour, respectively. The total fatality rate for this operation in the Husum, WA area is $F_{fat} \approx$ 8.7E-5 fatalities per flight hour. The value of $1/F_{fat}$ is perhaps a more intuitive value to analyze. This quantifies the number of flight hours to be expected until a fatality occurs. For forest, roads, towns, and fields, this value is approximately 640k, 280k, 14k, 70k hours until a fatality, respectively. The total flight time until an expected fatality is approximately 11k hours. It is interesting to note that although the flight operation is centered far away from the downtown area and urban areas make up only approximately 2% of the map, this is the area which is still the most likely to experience a fatality (most likely due to the extremely high relative population density). Also note that a fatality in a field is the next most likely occurrence (occurring once every 70k flight hours). Despite having an extremely low population density, the combination of no protection from collisions (D = 0) and the majority of the discrete PDF being clustered around fields yields a relatively high fatality rate (although this operation is still considered globally safe with a total expected fatality rate of once every 11k hours).

American Institute of Aeronautics and Astronautics

IV. Conclusions and Further Research

The methodologies outlined in this paper can be used to assess the risk of a UAS operating in a populated area. It allows the user to calculate the estimated number of bystander collisions per flight hour based on readily available data such as satellite imagery and census information. UAS failure rates can be determined from manufacturer specifications and experimentally obtained data such as hardware-in-the-loop simulation.

The tool is currently being used to develop safety cases which will be both illustrative and directly applicable to current issues. This analysis will be used for Aerovel's application to the FAA to obtain an experimental type certification for operations in the Husum, WA area. This work is also in the process of being applied to a case study to allow UAS to operate in the Juniper military operation area (MOA).

Current research is directed towards combining this methodology with existing tools[7] to assess the risk at different phases of the flight such as prolonged cruise. In addition, factors such as birdstrike and midair collisions are being added to the model. In addition, this analysis is valid for a single latitude/longitude/altitude point. Current research is directed towards extending this method to multiple locations and area. Various improvements to the current algorithm are also being investigated.

The probability density function in terms of both glide angle and crash distance are likely highly dependent on mode of operation. For example, thrust-borne maneuvers are likely to be highly unstable and once the in-flight computer fails, the aircraft crashes almost immediately. Conversely, in a stable wing-borne flight, the aircraft has the potential to glide for a considerable distance before crashing. Therefore, individual PDFs based on operating mode may improve accuracy of estimation by a significant margin.

Incorporating these elements will serve to ameliorate concerns about manned and unmanned aircraft coexisting in shared airspace.

V. Acknowledgements

References

[1] Anno, J., "Estimate of Human Control Over Mid-Air Collisions," *Journal of Aircraft*, Vol. 19, No. 1, 1982, pp. 86–88.

[2] McGeer, T., "Aerosonde Hazard Estimation," Aerovel Corporation.

[3] McGeer, T., "Safety, Economy, Reliability, and regulatory Policy for Unmanned Aircraft," .

[4] A. Lacher, A. Zeitlin, D. Maroney, K. Markin, D. Ludwig, and J. Boyd, "Airspace Integration Alternatives for Unmanned Aircraft," CAASD, The MITRE Corporation, Feb. 2010.

[5] Burke, D., *System Level Airworthiness Tool: A Comprehensive Approach to Small Unmanned Aircraft System Airworthiness*, Ph.D. thesis, North Carolina State University, 2010.

[6] Waggoner, B., *Developing a Risk Assessment Tool for Unmanned Aircraft Systems Operations*, Master's thesis, University of Washington, Seattle, WA, 2010.

[7] Lum, C. W. and Waggoner, B., "A Risk Based Pradigm and Model for Unamnned Aerial Vehicles in the National Airspace," *To appear in the proceedings of the 2011 Infotech@Aerospace Conference*, St. Louis, MO, March 2011.

[8] "Aerovel Begins Flight Test of Flexrotor Long-Endurance Robotic Aircraft with VTOL," Aerovel Press Release, http://www.aerovelco.com/papers/FlexrotorFirstFlightAnnouncement.pdf.

[9] McGraw, J., "AFS-400 UAS Policy 05-01, Unmanned Aircraft Systems Operations in the U.S. National Airspace System - Interim Operational Approval Guidance," Federal Aviation Administration.

[10] Sabatini, N., "Unmanned Aircraft Operations in the National Airspace System," Federal Aviation Administration.

[11] Davis, K., "Interim Operational Approval Guidance 08-01, Unmanned Aircraft Systems Operations in the U.S. National Airspace System," Federal Aviation Administration.

[12] Paskiewicz, F., "Order 8130.34: Airworthiness Certification of Unmanned Aircraft Systems," Federal Aviation Administration.

[13] Vuren, R. V., "Advisory Circular 91-57: Model Aircraft Operating Standards," Federal Aviation Administration.

[14] "STANAG 4671 Unmanned Aerial Vehicle Systems Airworthiness Requirements (USAR)," NATO Document, Sept. 2009.

[15] "Policy Statement Airworthiness Certification of Unmanned Aircraft Systems (UAS)," European Aviation Safety Agency (EASA), Aug. 2009.

[16] "FAA's NextGen Implementation Plan," Federal Aviation Administration.

[17] F. Martel, R.R. Schultz, W.H. Semke, Z. Wang, and M. Czarnomski, "Unmanned Aircraft Systems Sense and Avoid Avionics Utilizing ADS-B Transceiver," April 2009.

[18] "SAA Workshop Final Report: Sense and Avoid for Unmanned Aircraft Systems," Federal Aviation Administration.